DOI: 10.1002/ ((please add manuscript number))
Article type: Article

Reduced Recombination in High Efficiency Molecular Nematic Liquid Crystalline: Fullerene Solar Cells

Ardalan Armin, Jegadesan Subbiah, Martin Stolterfoht, Safa Shoaee, Zeyun Xiao, Shirong Lu, David J. Jones*, and Paul Meredith**

Dr. A. Armin, M. Stolterfoht, Dr. S. Shoaee, Prof. P. Meredith
Centre for Organic Photonics & Electronics (COPE), School of Mathematics and Physics and School of Chemistry and Molecular Biosciences, The University of Queensland, Brisbane 4072, Australia

E-mail: a.armin@uq.edu.au; djjones@unimelb.edu.au; meredith@physics.uq.edu.au
Dr. J. Subbiah, Dr. Z. Xiao, Dr. S. Lu, Dr. D. J. Jones
School of Chemistry, Bio21 Institute, The University of Melbourne, 30 Flemington Road, Parkville, Victoria 3010, Australia

Keywords: bulk heterojunction solar cells, bimolecular recombination, charge transfer state, non-Langevin, solar cells

Bimolecular recombination in bulk heterojunction organic solar cells is the process by which non-geminate photogenerated free carriers encounter each other, combine to form a charge transfer (CT) state which subsequently relaxes to the ground state. It is governed by the diffusion of the slower and faster carriers towards the electron donor: acceptor interface. In an increasing number of systems, the recombination rate constant is measured to be lower than that predicted by Langevin's model for relative Brownian motion and the capture of opposite charges. Herein, we investigate the dynamics of charge generation, transport and recombination in a nematic liquid crystalline donor: fullerene acceptor system that gives solar cells with initial power conversion efficiencies of >9.5%. Unusually, and advantageously from a manufacturing perspective, these efficiencies are maintained in junctions thicker than 300 nm. Despite finding imbalanced and moderate carrier mobilities in this blend, we observe strongly suppressed bimolecular recombination, which is ~150 times less than predicted by Langevin theory, or indeed, more recent and advanced models that take into account the

domain size and the spatial separation of electrons and holes. The suppressed bimolecular recombination arises from the fact that ground-state decay of the CT state is significantly slower than dissociation.

1. Introduction

Despite considerable activity directed towards materials development over the past two decades, there are still only a handful of organic semiconductor systems that deliver power conversion efficiencies (PCEs) >10% in single junction organic solar cells.[1] The so-called bulk heterojunction (BHJ) containing a blend of electron donor and acceptor organic semiconductors is the only architecture so far capable of delivering these single junction PCEs, and the electron acceptor is normally a fullerene such as $PC_{71}BM$ ([6,6]-phenyl-C71-butyric acid methyl ester). High efficiency donor materials are often polymers although there are a few notable exceptions.[2] One of the more interesting of these exceptions was recently reported by Sun et al. – a molecular nematic liquid crystalline donor with a benzo[1,2-*b*:4,5-*b*']dithiophene (BDT) centre and rhodamine end groups referred to as 'BTR'.[3] When combined with $PC_{71}BM$ in an optimised architecture, this material delivers an exceptionally high Fill Factor (FF ~ 0.75) and open circuit voltage (V_{OC} ~ 0.95) even when the heterojunction is 310 nm thick. This is unusual and important since 'thick junctions' (>200 nm) are advantageous from multiple perspectives for viable manufacturing of large area organic solar cells.

Electron and hole mobilities in non-crystalline organic semiconductors tend to be < 0.1 cm^2/Vs and often imbalanced by several orders of magnitude.[4] There has been significant effort towards understanding the impact of the efficiency with which photogenerated carriers are generated and extracted on the performance of thin and thick junction organic solar cells.[5-7] For example, Bartesaghi et al. showed how the FF of numerous organic donor:acceptor solar cell systems could be explained by only considering extraction (recombination) losses.[5] Armin et al. recently explained how inverting the junction electrical architecture can be used

to compensate for imbalanced mobilities in thick junction devices containing new high mobility donor polymers.[8] Further, Jin et al. demonstrated the direct relevance of suppressing recombination in large area organic solar cells to minimize the impact of thickness inhomogeneities.[9] There is also the question of how charge transfer state dissociation efficiency is related to the relative mobilities of the carriers.[10]

In general, increasing either the electron and hole mobilities or reducing the bimolecular recombination rate is a means to improving extraction efficiency – particularly in thick junctions. The disordered nature of BHJ films means that the former option is challenging, and been shown to not always deliver the expected benefits.[8] One is therefore led to consider as to how the latter could be achieved. In this regard, and noting the relatively disordered nature of organic semiconductors, the bulk bimolecular recombination rate constant of free charges, k_{bulk}, is traditionally considered to be dependent predominantly upon the time it takes for the carriers to diffuse close enough to each other to interact within their Coulomb radius. This leads to a diffusion-controlled recombination rate constant, k_L -

$$k_{\mathrm{L}} = (\mu_n + \mu_p)e/\epsilon\epsilon_0 \,, \tag{1}$$

where $\mu_{n(p)}$ is the electron (hole) mobility, e unit charge, ϵ the dielectric constant and ϵ_0 the vacuum permittivity. This construct was originally proposed for the recombination of ions by Langevin,[11] and has subsequently been widely used to describe the recombination of charges in disordered materials including dielectrics,[12] amorphous silicon,[13] small molecule organic semiconductors,[14] and polymers[15]. However, more than two decades ago it was shown by Arkhipov et al.[16] that in some semiconducting polymers, the experimental data for k_{bulk} does not agree with the predicted values of the Langevin rate, k_{L}. The origin of this anomaly was thought to be related to spatial separation of the potential landscapes that electrons and holes experience even in blends, *i.e.*, an effective phase separation of the two charge types.[17] A classic example of this phenomenon is the case of thermally annealed regioregular poly(3-

hexylthiophene):[6,6]-phenyl-C_{61}-butyric acid methyl ester (P3HT:PC_{61}BM) BHJs. Despite the P3HT:PC_{61}BM system only delivering PCEs of 3-5% (due to the relatively wide optical gap of P3HT), it has become an archetypal example of non-Langevin recombination. This system exhibits reduced bimolecular recombination rate ~100 times less than the Langevin rate[18], thus allowing the FF and PCE to be maintained at optimal values for heterojunctions three times thicker than for most other systems.[9] The reduction factor relative to the Langevin rate can be defined from equation 1 as follows:

$$\gamma_{\mathrm{L}} = \frac{k_{\mathrm{L}}}{k_{\mathrm{bulk}}} = \frac{(\mu_n+\mu_p)e}{\epsilon\epsilon_0 k_{\mathrm{bulk}}} \quad (2)$$

Whilst the benefits of reduced bimolecular recombination are now clear - and combining this feature with optimal light harvesting is an important strategy for increasing efficiencies in organic solar cells - the exact origins of non-Langevin recombination are widely debated, with only a few models proposed to explain the behaviour. For example, Tachiya et al. suggested that as free charges can recombine within their Coulomb radius,[19] the Langevin model which assumes that recombination occurs at a zero distance, is not a valid description in disordered semiconductors. Koster and Blom[20] postulated that the Langevin rate is not necessarily valid in the context of BHJs (which are multi-phase systems) since the faster carriers must wait for the arrival of the slower ones at the interface in order for recombination to occur. In such a scenario, the recombination rate constant can be reduced with respect to the Langevin rate when the electron/hole mobilities are strongly imbalanced. Counter to Equation 1, Groves et al.[21] used Monte-Carlo simulations, to show that the recombination rate in phase-separated systems is defined by the geometric mean of the electron and hole mobilities. Finally, and most recently, Heiber et al.[7] suggested that the origin of strongly reduced recombination is not necessarily an inherent property of the heterojunction i.e. the spatial separation of electrons and holes within different phases, however it could be true in extreme cases.[20] These workers showed that the so-called ‘encounter-limited’ recombination can only be suppressed to the

extent that it results in small reduction factors (< 10) for typical domain sizes (~5 – 10 nm) seen in high efficiency BHJs devices. According to their observations, the bimolecular recombination rate constant approaches the slower-carrier-limited rate as explained by Koster and Blom,[20] for very large domain sizes, whilst the rate constant approaches the faster-carrier-limited rate, as explained by Langevin, when the domain size is vanishingly small. Alternatively, within the framework of Onsager-Braun model for charge generation, the strongly reduced bimolecular recombination may be attributed to an efficient re-dissociation of CT states to free charges, which are in competition with their decay to the ground state; resulting in an equilibrium between the free charges and (a low population of) CT states. This scenario has recently been used by Burke et al. to analyse the equilibrium between the CT state and the charge-separated state populations and its implications for the open circuit voltage.[31] We will return to their findings later in the discussions.

Motivated by these debates, and the aforementioned unusual and potentially advantageous thick heterojunction performance of the BTR:$PC_{71}BM$ system, herein we have studied its recombination dynamics. We have used multiple methodologies to determine the bimolecular recombination reduction factor γ_L in optimised, high efficiency solar cells under operational conditions. Despite PCEs >9.5% being maintained for junction thicknesses up to 310 nm, we find nothing remarkable concerning the electron and hole mobilities (μ_e = 3×10^{-4} $cm^2V^{-1}S^{-1}$, μ_h = 4×10^{-3} $cm^2V^{-1}S^{-1}$), which are comparable to many other less efficient organic solar cell blend systems where the recombination rate is diffusion controlled.[4,5,22] We do however, observe a Langevin reduction factor of ~150 and this explains why high FF (~0.75) is maintained in thick junctions in this system. Furthermore, we determine that the free charge generation quantum yield is as high as 90%, implying efficient photogenerated charge transfer (CT) state dissociation. Importantly, by examining the relative rates within a simple Onsager-Braun construct, we also find that there is a high probability of CT state re-dissociation

following free carrier encounters at the donor: acceptor interface; this results in an equilibrium between CT states and free carriers. Hence, bulk bimolecular recombination is not limited by the encounter rate. The result is also consistent with the observed high open circuit voltages compared to the blend energy gap E_{DA}.

2. Results and Discussion

2.1. Solar cell performance

Figure 1a shows the molecular structure of the nematic liquid crystal electron donor material, BTR. Bulk heterojunction organic solar cells of BTR:$PC_{71}BM$ with the device structure as shown in **Figure 1b** were fabricated following the same processing conditions and methodologies as describe by Sun et al[3] and we confirm the originally reported efficiencies. Typical current density-voltage (*J-V*) curves for two active layer (heterojunction) thicknesses of 200 nm and 310 nm are shown in **Figure 1c** with PCEs of 9.4% and 9.5%, respectively. As previously indicated, the maintenance of performance in thick junctions is a matter of significant interest, and it has been shown that balanced charge carrier transport[23] and/or suppressed bimolecular recombination[6, 9] can both provide efficient charge extraction under such circumstances.

2.2. Electron and hole mobilities

The next phase of the study focused on the charge mobility of the blend film. A space charge limited current (SCLC) hole mobility of $\sim 10^{-3}$ cm^2/Vs has been previously reported for the BTR:$PC_{71}BM$ blend by Sun et al.[3] In the current work, we employ resistance dependent photovoltage (RPV), which is a more direct charge carrier mobility measurement methodology that is based upon extraction of electrons and holes in operational devices.[22] From the measured transit times as a function of the load resistance R_L (shown in **Figure 2**) and heterojunction thickness (310 nm), we obtain a faster carrier mobility of 4×10^{-3} $cm^2V^{-1}S^{-1}$ and

slower carrier mobility of 3 x 10^{-4} $cm^2V^{-1}S^{-1}$. We note that the value we obtain for the faster carrier mobility is close to the SCLC hole mobility reported by Sun et al.[3], and therefore we tentatively assign the faster carriers to the holes. Furthermore, the electron mobility is in agreement with those typically measured in a 50% by weight fullerene blends for multiple systems, which are consistently lower than that typically observed for blends with 80% fullerene loading (>10^{-3} $cm^2V^{-1}S^{-1}$).[4, 23]

This analysis indicates that charge carrier transport in the BTR:$PC_{71}BM$ system is not unusual from the perspective of carrier mobilities – both in terms of their magnitudes and the approximately 10 times imbalanced mobility. Hence, given the rather standard transport characteristics observed, one is led to suspect that favorable recombination is at the heart of the thick junction performance. This is consistent with Bartesaghi et al.,[5] who recently pointed out that the overall charge collection efficiency (which determines the FF and the PCE) is a result of the competition between recombination and charge extraction. In what is to follow, we study the recombination coefficient by applying 4 independent methods in steady state and transient modes, dark and illuminated.

2.3. Steady state current injection under equilibrium conditions

To quantify the bimolecular recombination reduction factor, we use operational BTR:$PC_{71}BM$ solar cells and analyze their *J-V* curves. In this regard, we assume an insulator (a semiconductor with low equilibrium carrier density) that is sandwiched between an anode and a cathode under forward bias. In the BTR:$PC_{71}BM$ device, the equilibrium charge carrier concentration is negligible compared to the magnitude of the charge on the electrodes at operational voltages. As such, the theory of double injection in insulators is applicable. If the recombination of charges is of Langevin-type, the recombination cross section is so large that the injected electrons and holes from the electrodes recombine as soon as they meet in space. The total

current (J_{SCL}) is hence the sum of the space charge limited (SCL) currents from the separated electrons and holes, (J_i^{SCL}) at the cathode and the anode respectively, given by [24]:

$$J_{\mathrm{SCL}} = J_n^{\mathrm{SCL}} + J_p^{\mathrm{SCL}} = \frac{9}{8}\epsilon\epsilon_0\left(\mu_n + \mu_p\right)\frac{V^2}{d^3}, \qquad \text{(for Langevin case).} \qquad (3)$$

Equation (3) is a generalized Mott-Gurney law and describes the maximum possible injected current into an insulator with the recombination rate limited to that given by the Langevin expression. However, if the recombination is reduced with respect to the diffusion-limited rate, the electron and hole SCL currents do not immediately annihilate each other upon meeting in space, rather allow for the establishment of a plasma in the bulk. In such a case, the current J_{DI} (herein referred to as the double injection current) can be calculated as shown by Mark and Lampert[25] (Equation 11.35)

$$J_{\mathrm{DI}} = \frac{9}{8}\epsilon\epsilon_0\mu_{\mathrm{eff}}\frac{V^2}{d^3}, \qquad (4)$$

where

$$\mu_{\mathrm{eff}} = \frac{2}{3}\left(4\pi\mu_f\mu_s\gamma_{\mathrm{L}}\right)^{1/2}. \qquad (5)$$

and μ_f and μ_s are respectively the faster and slower carriers. We have taken Equation (5) from the work of Mark and Lampert (Equation 11.35) and modified it to the notation of this work. To mitigate the voltage drop induced by the sheet resistance of the ITO electrode, we reduced the device area to 0.01 cm^2 from the original of 0.2 cm^2. **Figure 3** shows the *J-V* curves of these reduced area devices with fittings to the Parmenter-Ruppel expression using the mobility values of **Figure 2**. The best fit corresponds to a reduction factor of γ_{L} =150. Other fitting values are also shown to demonstrate the sensitivity of the results to the γ_{L} fitting. Note, the built-in voltage V_{bi} was approximated by the open circuit-voltage that matches up with the onset of the dark *J-V* curve as shown in the Supplementary Information. A static dielectric constant of 4 was determined using dark-charge extraction in linearly increasing voltage (dark-

CELIV) as previously described.[26] In the next section we employ equations (4) and (5) to quantify the reduction factor from the current transients.

2.4. Transient current injection

The double injection current methodology can also be performed in a transient mode.[6] The transient method benefits from normalization of the currents, implying that any injection barrier due to the imperfect contacts and/or series resistance will have a reduced impact on the analysis. When a forward bias voltage is applied to the solar cell, electrons and holes are injected from the cathode and the anode after an *RC*-decay that first charges the capacitor plates (the electrodes). We note that the *RC*-time must be minimized with respect to the other characteristic times of the system. After the *RC* decay, the total current is expected to be the sum of the two one-carrier SCL currents being injected from each electrode, *i.e.*, **Equation (3)**. As indicated above, when the two SCL currents meet in space, two scenarios can emerge: (i) a diffusion-limited recombination regime ($\gamma_{\mathrm{L}} = 1$) in which the recombination-cross-section is so high that the carriers immediately recombine and no plasma can be formed. In this case, the current does not increase with time and the transient current exhibits a plateau at its SCL value given by the generalized Mott-Gurney law, **Equation (3)**;[9] (ii) Alternatively in the case of suppressed recombination ($\gamma_{\mathrm{L}} > 1$), the current increases further when the carriers meet in space, and electron and hole density increase with time, forming a plasma within the bulk. In this case, the current ultimately increases to the value given by the Parmenter-Ruppel expression, **Equation (4)**. The rise of photocurrent is direct and unambiguous evidence of a suppressed recombination rate constant.[6] Note, that the double-injection current transient has been normalized to its initial value immediately after the *RC*-time. Normalizing **Equation (4)** by **Equation (3)** results in

$$\frac{J_{\mathrm{DI}}}{J_{\mathrm{SCL}}} = \frac{\mu_{\mathrm{eff}}}{\mu_n + \mu_p}, \tag{6}$$

which yields the reduction factor together with **Equation (3)**

$$\gamma_{\mathrm{L}} = \frac{9}{16\pi}\frac{(\mu_n+\mu_p)^2}{\mu_n\mu_p}\left(\frac{J_{\mathrm{DI}}}{J_{\mathrm{SCL}}}\right)^2. \quad (7)$$

Figure 4 shows the double injection current transient of an operational BTR:$PC_{71}BM$ solar cell (heterojunction thickness 310 nm) at a bias voltage of 2 V. The current saturates at $\frac{J_{\mathrm{DI}}}{J_{\mathrm{SCL}}} = 7$. Using the measured electron hole mobilities and **Equation (7)** we extract a reduction factor of $\gamma_{\mathrm{L}} = 135$ which is close to the value obtained from steady state *J-V* measurements.

2.5. Resistance dependent photocurrent transient

As discussed previously, systems with reduced bimolecular recombination can sustain higher carrier densities and as a result, a plasma can form during two-carrier injection. The same concept applies to photogenerated charges. To simulate this effect, we use a high fluence incident laser pulse which saturates the photovoltage and immediately screens the electric field inside the film. The photogenerated carriers either recombine due to diffusion, or are collected at the electrodes within the extraction time which can be controlled with a variable load resistance and associated *RC*-time of the circuit. If $\gamma_{\mathrm{L}} \gg 1$, then carriers can survive longer and more charges can be extracted. Integrating the photocurrent transient over time can therefore provide information about the reduction factor. The extracted charge saturates to a value *CV* at the largest load resistances because in this case, the *RC* time is much larger than the photocarrier lifetime, allowing only an amount of charge to be extracted equal to that capable of being stored on the electrodes. Reducing the *RC* time *via* the load resistance allows more charges to be extracted depending on the photocarrier lifetime and the bimolecular recombination coefficient. Using drift-diffusion modeling it has previously been shown that the amount of extracted charges versus the normalized *RC*-time obeys an empirical logarithmic expression[27]

$$\frac{Q_e}{CV} = 1 + c_1 \log\left[1 + c_2\left(\frac{RC}{t_{\mathrm{tr}}}\right)^{-c_3}\right], \quad (8)$$

where, the fitting coefficients are defined as

$$c_1 = 1.829\left(\gamma_{\mathrm{L}}^{-1} + 0.0159\gamma_{\mathrm{L}}^{-1/2}\right), \quad (9)$$

$$c_2 = 0.63\gamma_{\mathrm{L}}^{0.407}, \quad (10)$$

$$c_3 = 0.55\gamma_{\mathrm{L}}^{0.0203}, \quad (11)$$

The transit time in **Equation (8)** represents an effective transit time for the extraction of both electrons and holes $t_{\mathrm{tr}} = d^2/(\mu_s + \mu_f)V$. **Figure 5** shows the experimental results for the integrated photocurrent after a high fluence pulse excitation, *i.e.*, the amount of extracted charges normalized to the number of charges that can be stored on the electrodes (CV) plotted against t_{tr} normalized to the RC-time of the circuit. The fitting was based upon **Equation (8)**. A reduction factor of $\gamma_{\mathrm{L}} = 133$ is obtained which is again close to those values we evaluated based upon the double injection experiments. Non-matching parameters are also shown to highlight the sensitivity of the approach of the fitting parameters.

2.6. Intensity dependent photocurrent

To investigate the role of suppressed bimolecular recombination under operational conditions we utilized intensity dependent photocurrent (IPC) measurements. We have previously shown[9] that the critical photocurrent at which bimolecular recombination becomes significant is close to the slower carrier space charge current $J_{\mathrm{SCLC\,(slower)}} \approx CV/t_{\mathrm{tr\,(slower)}}$ for systems with Langevin recombination, and where $t_{\mathrm{tr\,(slower)}}$ denotes the transit time of the slower carriers. When the incident light intensity increases, the photocurrent also increases (initially linearly with light intensity) until the current reaches $J_{\mathrm{SCLC\,(slower)}}$. At this point, the charge in the device approaches CV and the average lateral spacing between the charge carriers reduces to a value at which their Coulombic attraction becomes larger than the external electric field that drives carriers to the electrodes. To avoid reaching the bimolecular recombination loss threshold (at the short circuit condition, at least) in Langevin-type systems such as PCDTBT:PC70BM,[9, 28] and under 1 sun illumination, the junction thickness must be kept thin

enough to avoid the formation of slower carrier space charges. Recently Stolterfoht et al.[29] have extended the use of the IPC methodology to non-Langevin systems and correlated the deviation point to both the slower carrier mobility, and the bimolecular recombination reduction factor. In this case, the current deviates at

$$J_{\mathrm{dev}} \approx \xi \frac{CV}{t_{\mathrm{tr(slower)}}} \gamma_L^{1/2}, \tag{13}$$

where, ξ is a prefactor which has been found to be approximately 0.4. Overall, **Equation (13)** is in line with double injection current transients in non-Langevin systems. If the recombination is suppressed, the slower carrier space charge limit is effectively increased by a factor of $\sqrt{\gamma_{\mathrm{L}}}$. Before moving on to the IPC results for BTR:$PC_{71}BM$ operational solar cells, we will further elaborate on the details of **Equation (13)** and its implications. As discussed in the **double injection current** section, non-Langevin recombination can increase the maximum injectable current into insulators. **Equation (6)** clearly shows that if $\gamma_{\mathrm{L}} > 1$, the double injection current can be enhanced from j_{SCLC} to j_{DI} whilst it is limited to j_{SCLC} if $\gamma_{\mathrm{L}} = 1$, and no rise in the transient will be expected. **Figure (6a)** shows the drift-diffusion simulation results of the intensity dependent photocurrent for a BTR:$PC_{71}BM$ solar cell (310 nm junction) with different Langevin reduction factors. In **Figure (6b)** simulated double injection transients for the same systems are shown at 2 V bias. It is clear that when $\gamma_{\mathrm{L}} = 1$, the injection current transient exhibits no rise from J_{SCLC} and as seen from the IPC plot in **Figure (6a)**, the photocurrent deviates at approximately $J_{\mathrm{SCLC\,(slower)}}$. By increasing the reduction factor ($\gamma_{\mathrm{L}} > 1$) the injection current exhibits a rise towards a maximum value of j_{DI}. Both j_{DI} and the deviation photocurrent (j_{dev}) increase with increasing reduction factor.

Figure 7 shows the experimental results of intensity dependent photocurrent measurements on a 310 nm thick BTR:$PC_{71}BM$ solar cell device at the short circuit condition. We obtain a deviation current of $J_{\mathrm{dev}} \approx 30\ \mathrm{mAcm^{-2}}$. Qualitatively, this deviation current is far larger than the slower carrier space charge limited current for a 310 nm thick BTR:$PC_{71}BM$ device

($j_{\mathrm{SCLC}}(310\ \mathrm{nm}) \approx 3.5\ \mathrm{mAcm}^{-2}$). We can use **Equation (11)** to quantify the reduction factor from J_{dev} and the slower carrier mobility. Using an internal voltage that is approximately the same as the open circuit voltage (~0.9 V) and a dielectric constant of 4, we calculate $\gamma_{\mathrm{L}} \approx 150$. Hence, using four different methodologies to measure the reduction factor we see clearly that the recombination in BTR:$PC_{71}BM$ is approximately 150 times suppressed with respect to that predicted by the Langevin model.

2.7. Origin of the suppressed recombination and its implications

We now discuss charge generation in these high efficiency BTR:$PC_{71}BM$ solar cells and its inter-relation with the observed non-Langevin recombination. **Figure 8(a)** shows the optical constants; refractive index and extinction coefficient of BTR:$PC_{71}BM$ films on glass. Using these parameters and the optical constants of all the ancillary layers in the solar cell stack, we were able to quantify the parasitic absorptions (i.e. optical losses) in the full device. Subsequently, using the external quantum efficiency (EQE) and near normal incidence reflection we evaluated the internal quantum efficiency (IQE).[30] The IQE was found to be ~90% [junction thickness 310 nm, **Figure 8(b)**] and virtually flat as expected, across the absorption window. We note that the photocurrent does not deviate from linearity in this system until high light irradiances – five orders of magnitude larger than the light irradiance we used to measure the EQE (~ 1 μW/cm^2) in **Figure (6)**. It has recently been shown that under these conditions, the IQE is not limited by non-geminate recombination losses (*i.e.*, bimolecular losses or trap-assisted non-geminate recombination in the bulk) and therefore, it reflects the charge generation quantum yield.[10] Hence, the measurements show that charge generation for the BTR:$PC_{71}BM$ blend is very efficient, and indicate that charge generation and recombination are inter-related. The probability of ionization of CT states is given by the branching ratio $P = k_d/(k_f + k_d)$, where k_d is the rate constant for dissociation of CT to charge separated

(CS) states, and k_f is the decay rate constant of the CT to the ground state (GS). When $k_d >> k_f$, efficient charge generation is expected. Further increasing the ratio of k_d/k_f results in a saturation of the CT state dissociation probability, and will not further increase the charge generation. However, this leads to the formation of an equilibrium between CT and CS states and overall, lowers the CT states density and their recombination rate. The bimolecular recombination involves two independent stages. The first rate, k_{enc}, depends on the probability of the encounter between a free electron and a free hole to form a CT state with a diffusion-limited rate constant. The second stage is the recombination of the CT states to the ground state. The bulk recombination rate constant can therefore be written as

$$k_{\mathrm{bulk}} = (1 - P)k_{\mathrm{enc}} \,. \tag{14}$$

The bulk recombination and Langevin rate constants are related via $\gamma_L = k_L/k_{\mathrm{bulk}}$ and therefore we can write for γ_L

$$\gamma_L = \gamma_{\mathrm{CT}}\gamma_{\mathrm{enc}}. \tag{15}$$

where $\gamma_{\mathrm{enc}} = k_L/k_{\mathrm{enc}}$ and $\gamma_{\mathrm{CT}} = \frac{1}{1-P}$.

In **Figure (9)** we have plotted the predicted diffusion limited reduction factors (γ_{enc}) for different domain sizes - based on the model of Heiber et al.[7] - versus the square root of the mobilities product assuming an electron mobility of 3 x 10^{-4} $cm^2V^{-1}s^{-1}$. In addition, we also plot the slower-carrier-limited rate constants according to Koster and Blom,[20] as well as the harmonic mean and the geometric mean as suggested by Groves and Greenham.[21] Plotting the measured reduction factor ($\gamma_L \sim 150$) of the BTR:$PC_{71}BM$ system on the same figure demonstrates that this reduction factor is significantly larger than that predicted by any of these three models, regardless of the domain size or the nano-morphology. This implies that the origin of non-Langevin recombination in this material system is predominantly because of the

high probability of CT state dissociation (P ≫1). If we consider a domain size of 10 nm, then γ_{enc}~2, which implies $\gamma_{\mathrm{CT}} = \frac{k_d}{k_f}$~75%.

In addition to these beneficial effects of the strongly reduced recombination rate for the charge generation yield, Burke et al.[31] have demonstrated that a long CT state lifetime (which corresponds to large $k_d\ /k_f$ and reduced recombination) is highly desirable to increase the open-circuit voltage of organic solar cells by the reducing energy losses associated with non-radiative charge recombination. A weak coupling of the CT states to the ground state is a key to achieving this condition whereby this reduces the radiative V_{OC} loss logarithmically.[31] It has also been shown that many solar cells lose between 300 to 700 meV in $\mathrm{eV_{OC}}$ compared to the CT state energy (or approximately the blend energy gap), as determined by the difference of the ionization potential of the donor and the electron affinity of the acceptor minus the CT state binding energy $\mathrm{E_{b(CT)}}$. We note that the exact energy and binding energy of BTR:$PC_{71}BM$ CT states are not known here and therefore, we are not able to calculate the exact $\mathrm{V_{OC}}$ loss. Nevertheless, a Langevin reduction factor of 150 corresponds to a reduction of the $\mathrm{V_{OC}}$ loss (i.e. an increased$\mathrm{V_{OC}}$) of $k_B\mathrm{Tln}(\frac{1}{150}) \approx 120$ meV with respect to a Langevin system with identical energy levels as BTR:$PC_{71}BM$. Here k_B is the Boltzmann constant and T the absolute temperature. This is perhaps the reason for the respectable open circuit voltage of 0.94 V with energy levels similar to many other donor/acceptor systems[3,32] which exhibit lower $\mathrm{V_{OC}}$.

3. Conclusion

Bulk heterojunction organic solar cells based upon the BTR:$PC_{71}BM$ blend system exhibit state-of-the-art power conversion efficiencies exceeding 9.5%. These efficiencies are maintained in 'thick' heterojunction devices (> 300 nm). We have found that the electron and hole transport properties in optimized BTR:$PC_{71}BM$ operational solar cells do not explain this behaviour – the magnitude and ratio of the mobilities are typical of numerous high and

moderate efficiency organic solar cell BHJ combinations. We found a mobility imbalance of ~10 and strongly suppressed bimolecular recombination with respect to the values predicted by Langevin theory that cannot be explained by the carriers existing in separate phases. To quantify the bimolecular recombination reduction factor, we employed four independent methods, which are based on injection and extraction of charges in both steady state and transient regimes. The results obtained from all four methods are in strong agreement, confirming a reduction factor of ~150 in this intriguing molecular nematic liquid crystal donor: fullerene acceptor system. The simultaneous presence of high free charge generation quantum yield and suppressed bimolecular recombination, suggests a low recombination rate of the CT states compared to the dissociation rate. The suppressed CT state recombination also contributes to the high V_{OC} in this system that is only ~ 100 meV smaller than the blend optical gap. Our results explain why this BTR:$PC_{71}BM$ system works so well in organic solar cells, and potentially delivers new design strategies to suppress the CT state recombination, which simultaneously optimises all photovoltaic key parameters of organic solar cells.

4. Experimental Section

Materials: $PC_{71}BM$ was purchased from American Dye Source and used without purification. BTR was synthesised in house based on the methodology previously described.[3]

Solar cell fabrication: Solar cells were fabricated on pre-patterned indium tin oxide (ITO) glass substrates (15 Ω sq^{-1}: Xinyan) in a class 1000 clean room. The substrates were cleaned in a detergent bath (Alconox) at 80 °C for 10 min and mechanically cleaned by a soft cloth, followed by sonication in sequence with Alconox, deionized water, acetone, and 2-propanol for 10 min each. The cleaned substrates were dried with nitrogen before spin-coating the

subsequent layers. Substrates were 2.5 cm x 2.5 cm with 6 pixels of 0.2 cm^2 each. The cleaned substrates were coated with a 30±5 nm layer of poly(3,4-ethylenedioxythiophene):poly(styrenesulfonate) (PEDOT:PSS) purchased from Heraeus (Clevios P Al4083), by spin-coating at 5000 rpm for 60 s. The PEDOT:PSS layer was baked for 10 min at 170 °C. After cooling, the substrates were transferred into a nitrogen-filled glove box for device fabrication (O_2 <1 ppm, H_2O <1 ppm). After that, BTR:$PC_{71}BM$ films were deposited from the solutions described above on top of the PEDOT:PSS layer in a nitrogen atmosphere with oxygen and water concentration of <5 ppm. Individual solutions of BTR and $PC_{71}BM$ were prepared in anhydrous chloroform at room temperature and at a concentration of 40 mg/mL. The solutions were then mixed at a volume ratio of 1:1 and spin-coated at 1000 rpm to achieve an active layer thickness of ~310 nm as determined with a Veeco Dektak 150 profilometer. Total concentration of 30 mg/mL was used in order to make 200 nm thick films. The films were then treated with solvent annealing and finished with thermal evaporation of a Ca/Al cathode (20 nm and 80 nm) under a 10^{-6} mbar vacuum.

Solvent annealing: Solvent annealing was performed in a nitrogen glove box with conditions O_2 <1 ppm and H_2O <1 ppm. Tetrahydrofuran (1.5 mL) was injected into a glass Petri dish (volume 40 mL radius 5 cm). The Petri dish was closed for 2 min to let the vapour saturate the inner atmosphere. Then BTR:$PC_{71}BM$ films were attached on the back side of the Petri dish lid, which was quickly swapped with the lid covering the solvent containing Petri dish. The film was about 1 cm above the solvent level during the annealing. After 15 sec the film was removed from the petri dish.

Solar cell characterization: Current-density–voltage (*J-V*) characteristics were acquired in a nitrogen glove box with conditions O_2 <1 ppm and H_2O <1 ppm using a Keithley 2400 Source Measure Unit under simulated Air Mass 1.5 Global (AM 1.5 G) 1000 W/m^2 illumination (as determined by an NREL-certified photodiode with a KG5 filter) provided by an Abet Sun 2000

Solar Simulator. EQE and near normal incidence reflection spectrum were measured with a QEX7 setup from PV Measurements Inc., using a calibrated photodiode. The integrated EQEs were within ±10% of short circuit current as a self-consistent measure of system calibration.

Internal quantum efficiency: The IQEs was determined using a previously reported methodology.[30] The optical constants of the BTR:$PC_{71}BM$ blends were determined using a combination of spectroscopic ellipsometry (J. A. Woollam VUV-VASE ellipsometer) and reflectometry (QEX7 setup from PV Measurements Inc) based upon a previously reported approach.[33] The optical constants of all the non-active layers have been reported elsewhere.[34]

Steady state and transient double injection: Double injection current-voltage curves were recorded in the dark using a Keithley 2400 Source Measure Unit. The double injection current transients were measured using an Agilent 33250A arbitrary waveform generator synchronised by a Stanford Research Systems DG535 delay generated. The signal was recorded using a digital storage oscilloscope (LeCroy Waverunner A6200) via a LabVIEW code.

Resistance dependent photovoltage: Photocurrent and photovoltage transients were recorded using the same setup as explained for double injection transients. A pulsed second-harmonic Nd:YAG laser (Quantel Brio) working at 532 nm was used with pulse duration of 5 ns. The laser beam with ~50 mJ energy output was attenuated with a natural optical-density (OD) filter set. Low laser pulse fluences (~OD 7) were used for the RPV mobility measurements in order to prevent a redistribution (screening) of the internal electric field and maintaining quasi-short-circuit conditions regardless of the load resistance. In contrast, a high laser fluence (~OD 3.5) was used to measure the bimolecular recombination coefficient on the same devices.

Intensity dependent photocurrent: Light intensity dependent photocurrents, EQEs, and *J–V* curves were determined using a second harmonic Nd:YAG laser (Laserver) operating continuously at 532 nm as the illumination source, with a series of neutral density filters purchased from Thorlabs and Holmarc used to vary the light intensity. The light intensity was

calibrated using a calibrated photodiode. The photocurrent was recorded by an Agilent B1500A Semiconductor Analyser.

Acknowledgements
This Program was funded by the Australian Government through the Australian Renewable Energy Agency (ARENA) Australian Centre for Advanced Photovoltaics (ACAP). Responsibility for the views, information or advice expressed herein is not accepted by the Australian Government. This work was performed in part at the Queensland node of the Australian National Fabrication Facility (ANFF) - a company established under the National Collaborative Research Infrastructure Strategy to provide nano and micro fabrication facilities for Australia's researchers. The Centre for Organic Photonics and Electronics is a strategic initiative of the University of Queensland.

Received: ((will be filled in by the editorial staff))
Revised: ((will be filled in by the editorial staff))
Published online: ((will be filled in by the editorial staff))

[1] Z. He, B. Xiao, F. Liu, H. Wu, Y. Yang, S. Xiao, C. Wang, T. P. Russell, Y. Cao, Nature Photonics 2015, 9, 174.
[2] Q. Zhang, B. Kan, F. Liu, G. Long, X. Wan, X. Chen, Y. Zuo, W. Ni, H. Zhang, M. Li, Nature Photonics 2015, 9, 35.
[3] K. Sun, Z. Xiao, S. Lu, W. Zajaczkowski, W. Pisula, E. Hanssen, J. M. White, R. M. Williamson, J. Subbiah, J. Ouyang, A. Holmes, W. W. H. Wong and D. Jones, Nature communications 2015, 6, 6013..
[4] A. Armin, G. Juska, M. Ullah, M. Velusamy, P. L. Burn, P. Meredith, A. Pivrikas, Advanced Energy Materials 2014, 4, 1300954.
[5] D. Bartesaghi, I. del Carmen Pérez, J. Kniepert, S. Roland, M. Turbiez, D. Neher, L. J. A. Koster, Nature communications 2015, 6, 7083.
[6] A. Armin, G. Juska, B. W. Philippa, P. L. Burn, P. Meredith, R. D. White, A. Pivrikas, Advanced Energy Materials 2013, 3, 321.
[7] M. C. Heiber, C. Baumbach, V. Dyakonov, C. Deibel, Physical review letters 2015, 114, 136602.
[8] Ardalan Armin, A. Yazmaciyan, Mike Hambsch, Paul L. Burn and Paul Mederdith, ACS Photonics 2015, 2, 1745-1754.
[9] H. Jin, A. Armin, M. Hambsch, Q. Lin, P. L. Burn, P. Meredith, physica status solidi (a) 2015, 212, 2246-2254
[10] M. Stolterfoht, B. Philippa, S. Shoaee, H. Jin, W. Jiang, R. D. White, P. L. Burn, P. Meredith, A. Pivrikas, The Journal of Physical Chemistry C 2015, 119, 26866.
[11] P. Langevin, Ann. Chim. Phys 1903, 28, 122.
[12] V. Arkhipov, I. Perova, Journal of Physics D: Applied Physics 1993, 26, 1301.
[13] B. Reis, H. Bassler, G. Schonherr, M. Silver, E. Snow, Journal of Non-Crystalline Solids 1984, 66, 243; E. Schiff, Journal of non-crystalline solids 1995, 190, 1.
[14] A. McGhie, H. Blum, M. Labes, Molecular Crystals and Liquid Crystals 1969, 5, 245.
[15] R. Hughes, The Journal of Chemical Physics 1973, 58, 2212.
[16] V. Arkhipov, I. A. Perova, A. Rudenko, International journal of electronics 1992, 72, 99; A. Twtnev, A. Karpechin, S. Boev, V. Saenko, E. Pozhidaev, physica status solidi (a) 1992, 132, 163.
[17] G. Adriaenssens, V. Arkhipov, Solid state communications 1997, 103, 541.

[18] G. Juška, K. Arlauskas, J. Stuchlik, R. Österbacka, Journal of non-crystalline solids 2006, 352, 1167.
[19] M. Hilczer, M. Tachiya, The Journal of Physical Chemistry C 2010, 114, 6808.
[20] L. Koster, V. Mihailetchi, P. Blom, Applied physics letters 2006, 88, 052104.
[21] C. Groves, N. Greenham, Physical Review B 2008, 78, 155205.
[22] M. Stolterfoht, B. Philippa, A. Armin, A. K. Pandey, R. D. White, P. L. Burn, P. Meredith, A. Pivrikas, Applied Physics Letters 2014, 105, 013302.
[23] A. Armin, M. Hambsch, P. Wolfer, H. Jin, J. Li, Z. Shi, P. L. Burn, P. Meredith, Advanced Energy Materials 2014, 5, 1401221.
[24] R. H. Parmenter, W. Ruppel, Journal of Applied Physics 1959, 30, 1548.
[25] M. A. Lampert, P. Mark, *Current injection in solids*, Academic Press, 1970.
[26] A. Armin, M. Velusamy, P. L. Burn, P. Meredith, A. Pivrikas, Applied Physics Letters 2012, 101, 083306.
[27] B. Philippa, M. Stolterfoht, R. D. White, M. Velusamy, P. L. Burn, P. Meredith, A. Pivrikas, The Journal of chemical physics 2014, 141, 054903.
[28] T. M. Clarke, J. Peet, A. Nattestad, N. Drolet, G. Dennler, C. Lungenschmied, M. Leclerc, A. J. Mozer, Organic Electronics 2012, 13, 2639.
[29] M. Stolterfoht, A. Armin, B. Philippa, R. D. White, P. L. Burn, P. Meredith, G. Juska, A. Pivrikas, Sci. Rep. 2015, 5, 9949.
[30] A. Armin, M. Velusamy, P. Wolfer, Y. Zhang, P. L. Burn, P. Meredith, A. Pivrikas, Acs Photonics 2014, 1, 173.
[31] T. M. Burke, S. Sweetnam, K. Vandewal, M. D. McGehee, Advanced Energy Materials 2015, 5, 1500123.
[32] A. Armin, I. Kassal, P. E. Shaw, M. Hambsch, M. Stolterfoht, D. M. Lyons, J. Li, Z. Shi, P. L. Burn, P. Meredith, Journal of the American Chemical Society 2014, 136, 11465.
[33] Q. Lin, A. Armin, R. C. R. Nagiri, P. L. Burn, P. Meredith, Nature Photonics 2014, 9, 106-112.
[34] D. M. Lyons, A. Armin, M. Stolterfoht, R. C. Nagiri, R. D. Jansen-van Vuuren, B. N. Pal, P. L. Burn, S.-C. Lo, P. Meredith, Organic Electronics 2014, 15, 2903.

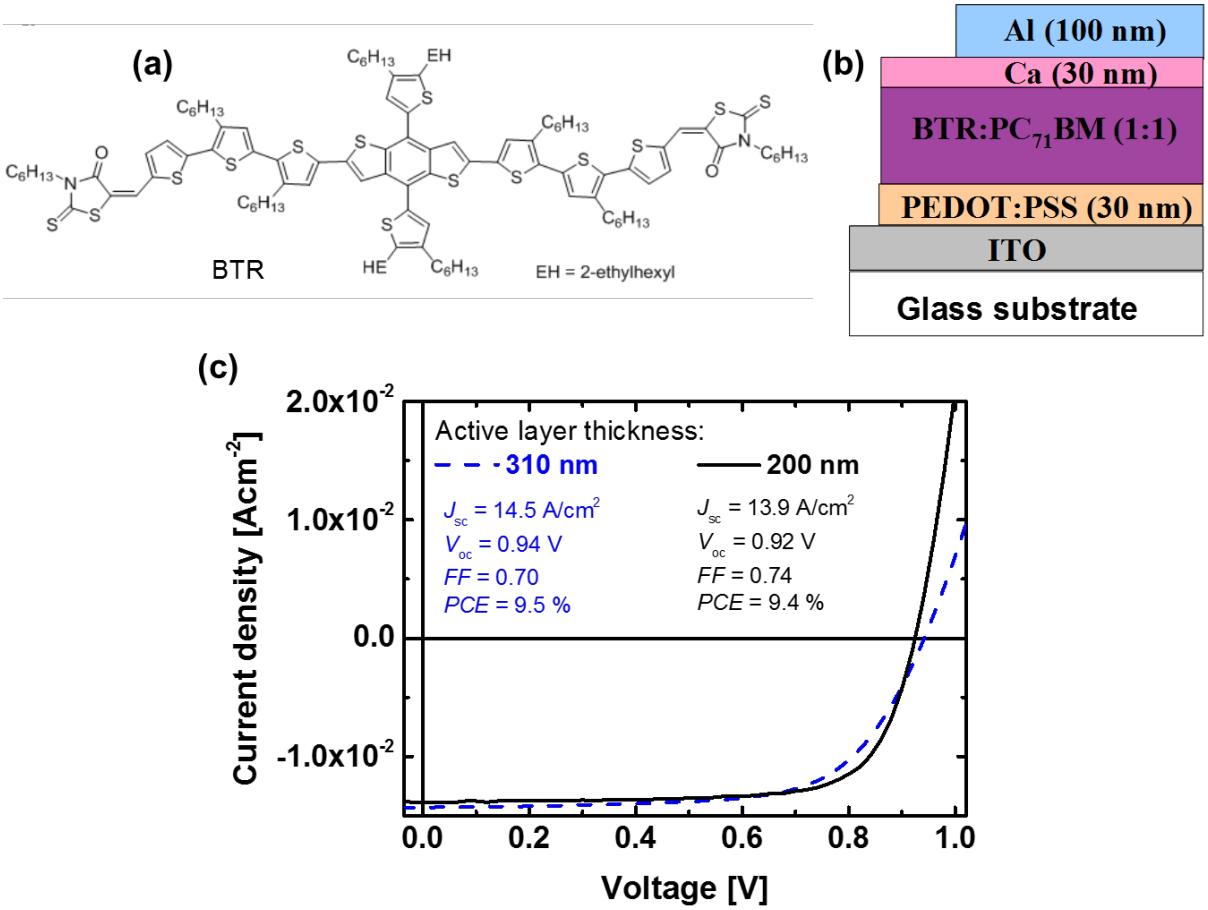

Figure 1. Device structure and the performance of BTR:$PC_{71}BM$ organic solar cells. (a) Molecular structure of BTR. (b) Device structure of the solar cell devices made and characterized. (c) Current-voltage curves of BTR:$PC_{71}BM$ solar cells with junction thicknesses of 200 nm and 310 nm, respectively, measured under AM1.5G illumination conditions.

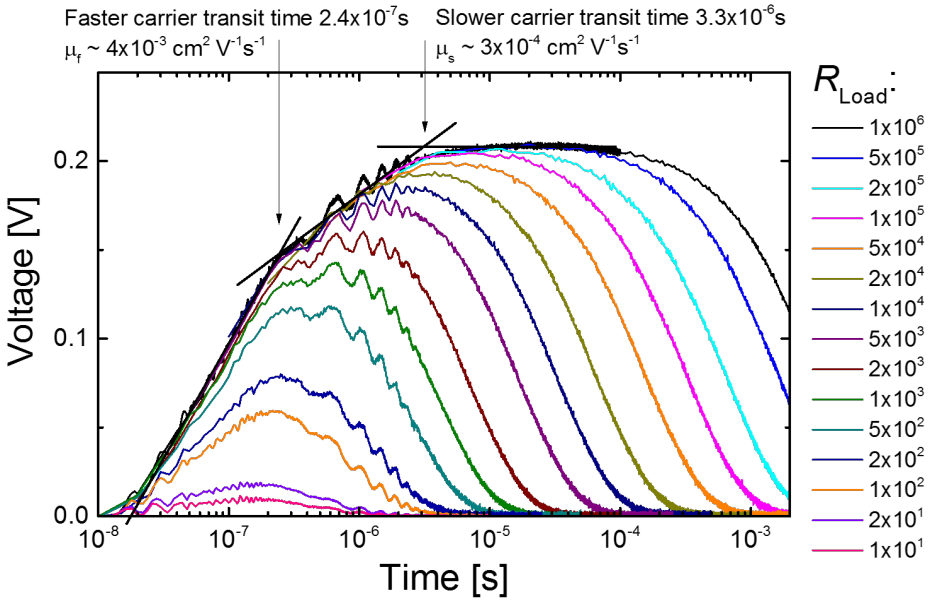

Figure 2. Resistant dependent photovoltage transients of a BTR:$PC_{71}BM$ solar cell at low laser light intensity. The electron and hole mobilities are quantified from their corresponding transit times marked on the figure.

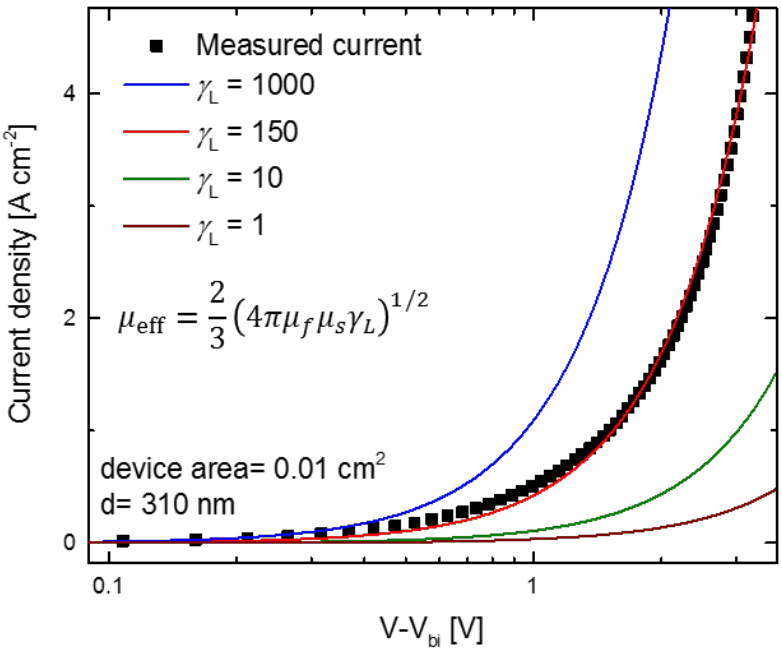

Figure 3. Current density versus effective voltage for a BTR:$PC_{71}BM$ solar cell (310 nm junction thickness, device area 0.01 cm^2 and static dielectric constant of 4). (a) Parmenter-Ruppel current fittings based upon the effective mobility from **Equation (5)** for different values of γ_L. The best fit can be achieved with a Langevin reduction factor of $\gamma_L = 150$.

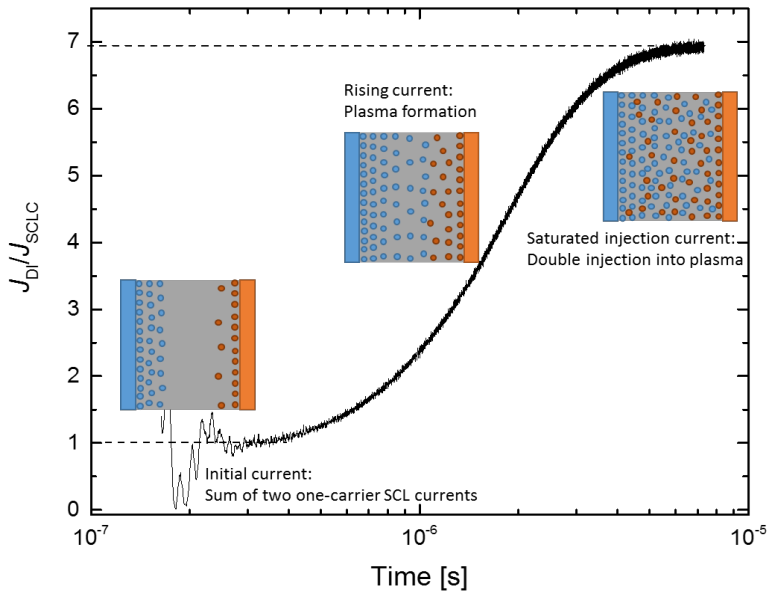

Figure 4. Injection current transient at forward bias voltage of 2 V normalized to the initial space charge limited (SCL) current. Inset cartoons show the injection of the initial one-carrier SCL currents near the anode and the cathode, rising carrier densities in line with rising current, and ultimately a saturated double injection current into the built-up plasma. The normalized current value of approximately 7 corresponds to a Langevin reduction factors of 135 based upon **Equation (7)**.

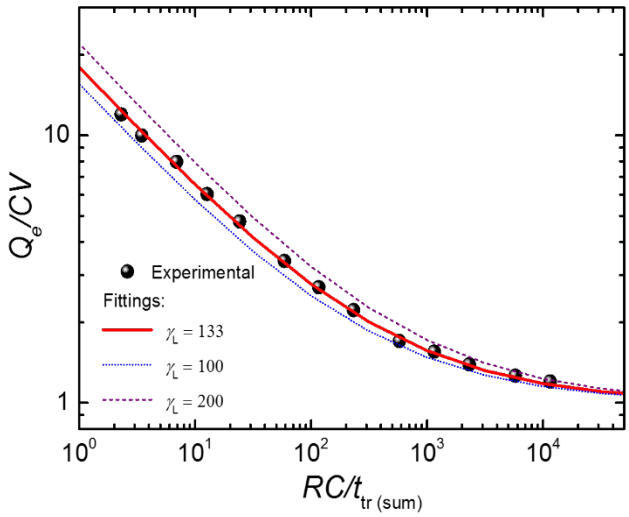

Figure 5. Extracted charge normalized to the amount of charge on the electrodes (CV) versus the faster carrier transit time normalized to the RC-time. The photovoltage transients (devices similar to **Figure 1**) are measured at high laser fluences that saturate the photovoltage (number of photons $\gg$ CV/e) and subsequently integrated to obtain the extracted charge. The experimental results are in agreement with the results from injection based methods [**Equation (7)**], *i.e.*, $\gamma_{\mathrm{L}} = 133$. The dashed purple and dotted blue lines correspond to non-matching fittings in order to show the sensitivity of the fittings to the γ value.

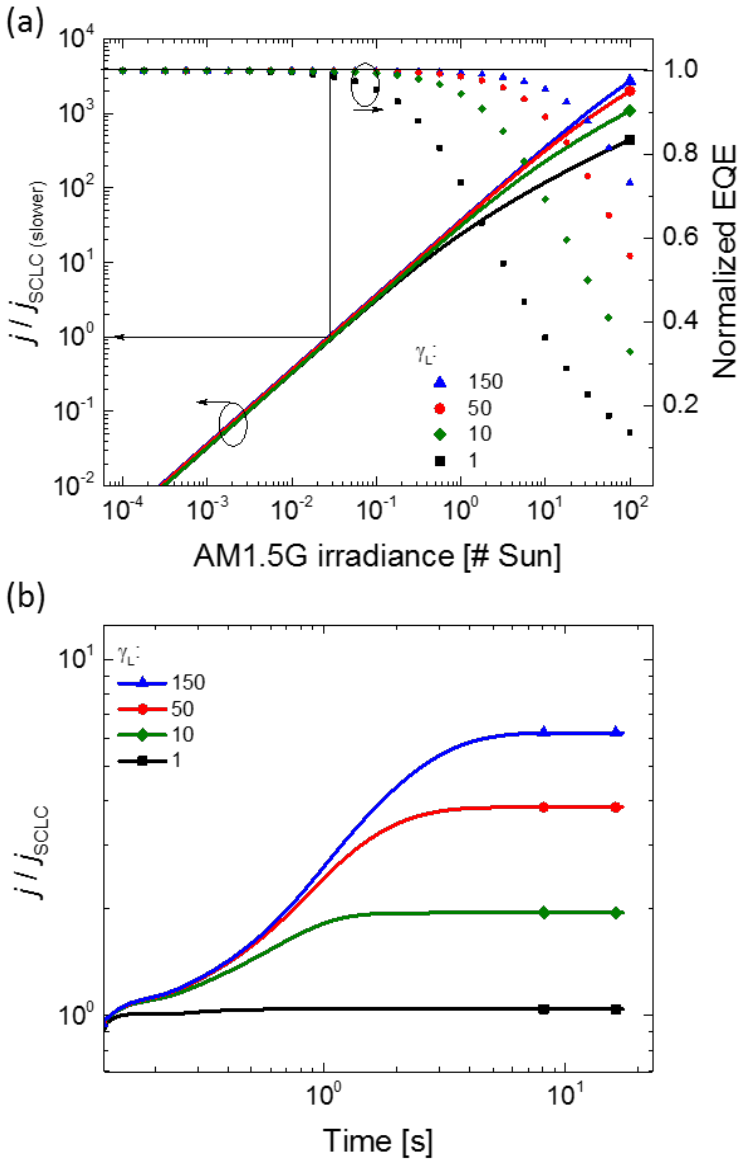

Figure 6. (a) Simulated intensity dependent photocurrent for a BTR:$PC_{71}BM$ solar cell with active layer thickness of 310 nm under short circuit condition for different Langevin reduction factors. The current is normalized to the slower carrier space charge current (SCLC). By increasing the reduction factor, the photocurrent deviates at photocurrent values larger than the slower carrier SCLC. The deviation points are more visible from the normalized external quantum efficiencies (EQEs). (b) Simulated double injection transients for the same device at a forward bias voltage of 2 V. In all cases the injection current starts from the SCLC limit. For larger reduction factors the current reaches significantly higher values.

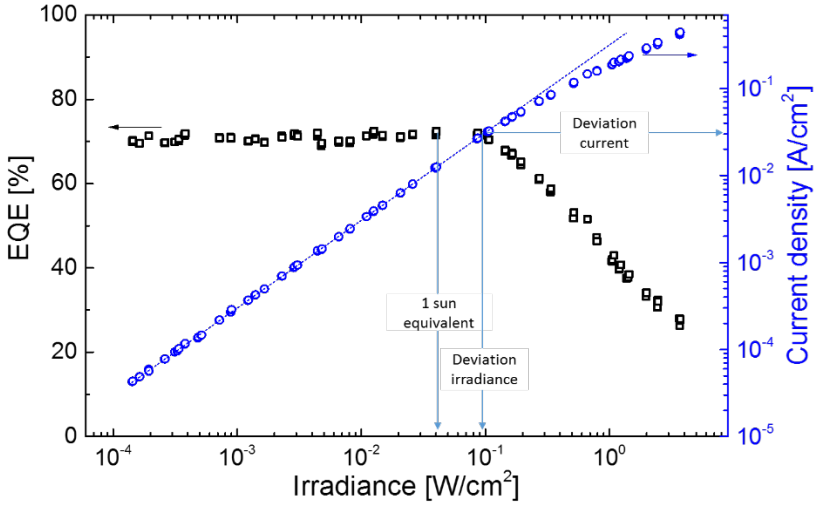

Figure 7. The photocurrent (right axis) versus continuous light irradiance at an incident wavelength of 532 nm for a BTR:$PC_{71}BM$ solar cell with a junction thickness of 310 nm under short circuit conditions. The EQE is plotted on the left axis versus irradiance to better visualize the irradiance at which the photocurrent deviates from linearity, which also leads to a decrease in the EQE. Due to suppressed bimolecular recombination, the deviation happens at a photocurrent of ~0.03 A/cm^2, which is larger than the space charge current of the slower carriers. A reduction factor of $\gamma_L = 150$ can be estimated from the deviation current and based upon **Equation (13)**.

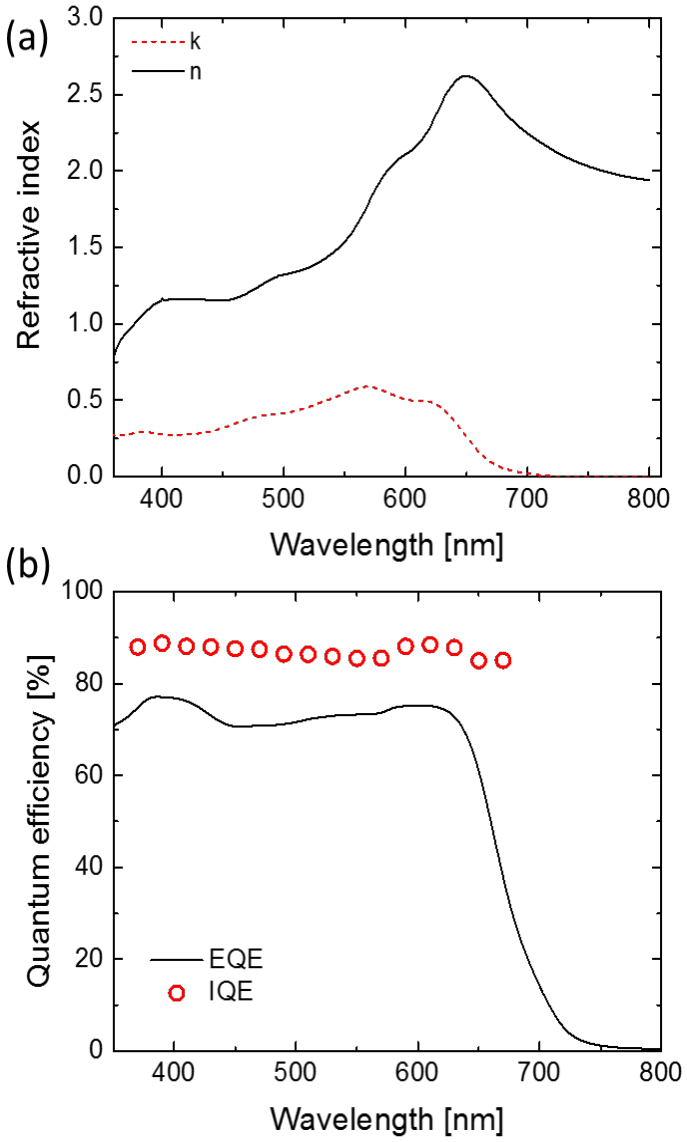

Figure 8. (a) Optical constants (n, k) of a BTR:$PC_{71}BM$ film as determined by spectroscopic ellipsometry and reflectometry. (b) Internal and external quantum efficiencies of BTR:$PC_{71}BM$ solar cells. The IQE is measured at low light irradiance where non-geminate recombination is absent. Therefore, the IQE reflects the charge generation quantum yield which is ~ 90%.

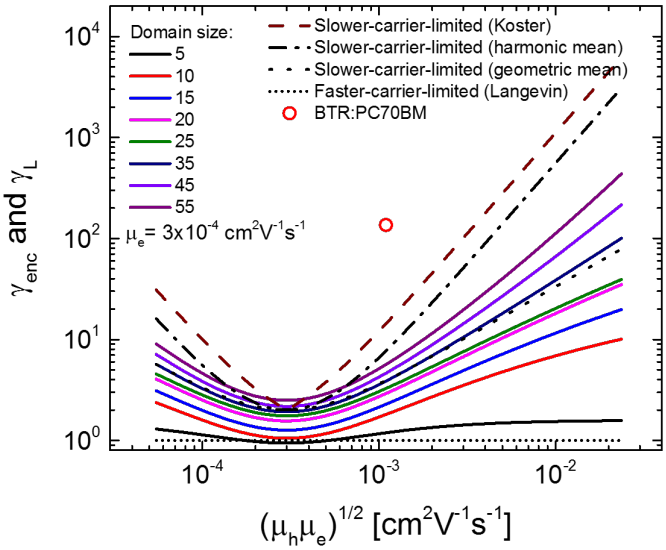

Figure 9. Predicted diffusion controlled reduction factors of the bimolecular recombination for different domain sizes (colored lines, calculated based on Heiber et al.[7]) as a function of the square root of the mobilities assuming an electron mobility of 3 x 10^{-4} $cm^2V^{-1}s^{-1}$, compared to predictions of empirical models such as the slower-carrier-limited rate constant, the harmonic and geometric mean (dashed lines). All these models assume a diffusion (encounter) limited recombination mechanism. The measured Langevin reduction factor of BTR:$PC_{71}BM$ (~150) is plotted as a red circle, demonstrating the strongly reduced recombination compared to all of these models.